ACS APPLIED MATERIALS & INTERFACES

Research Article

www.acsami.org

Growth Mechanism of Pulsed Laser Fabricated Few-Layer MoS_2 on Metal Substrates

Tamie A. J. Loh and Daniel H. C. Chua*

Department of Materials Science and Engineering, National University of Singapore, Singapore 117576

ABSTRACT: Pulsed laser deposition (PLD) on metal substrates has recently been discovered to present an alternative method for producing highly crystalline few-layer MoS_2. However, not every metal behaves in the same manner during film growth, and hence, it is crucial that the ability of various metals to produce crystalline MoS_2 be thoroughly investigated. In this work, MoS_2 was deposited on metal substrates, Al, Ag, Ni, and Cu, using a pulsed laser. Highly crystalline few-layer MoS_2 was successfully grown on Ag, but is absent in Al, Ni, and Cu under specific growth conditions. This discrepancy was attributed to either excessively strong or insufficient adlayer−substrate interactions. In the case of Al, the effects of the strong interface interactions can be offset by increasing the amount of source atoms supplied, thereby producing semicrystalline few-layer MoS_2. The results show that despite PLD being a physical vapor deposition technique, both physical and chemical processes play an important role in MoS_2 growth on metal substrates.

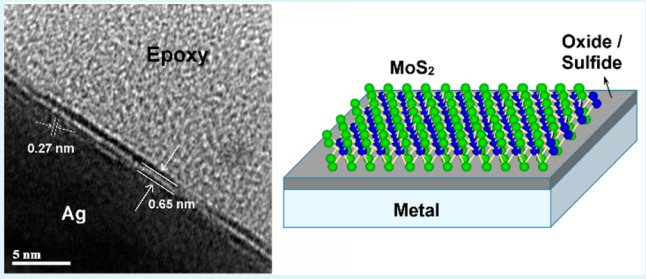

KEYWORDS: *pulsed laser, few-layer MoS_2, X-ray photoelectron spectroscopy, metal support, conventional epitaxy*

1. INTRODUCTION

Within the emerging class of ultrathin two-dimensional (2D) layered materials, graphene has undoubtedly attracted the most attention due to its remarkable mechanical[1] and electronic properties.[2] However, the intrinsic limitations of graphene such as the lack of a band gap necessary for efficient high performance field effect transistors (FETs) has motivated research on other 2D materials. One such material is molybdenum disulfide (MoS_2), from the family of layered transition metal dichalcogenides (LTMDs). Unlike metallic graphene, MoS_2 is an indirect band gap semiconductor with an energy gap of 1.2 eV in bulk form.[3] But when thinned down to a monolayer, quantum confinement effects gives rise to an indirect-to-direct transition such that single layer MoS_2 possesses a direct gap of 1.9 eV.[4,5] This leads to an enhancement in photoluminescence of single layer MoS_2, making the material attractive for use in optoelectronic devices. In addition, transistors based on atomically thin MoS_2 present impressive carrier mobilities of 200−500 $cm^2/(V\ s)$ and excellent on/off current ratios, which render them suitable for next generation electronic devices.[6,7]

One of the key challenges in MoS_2 research is the fabrication of high quality ultrathin films. Conventional "top-down" techniques such as mechanical exfoliation[8,9] and solvent based exfoliation[10,11] are time-consuming, are not scalable, and produce flakes that are not thickness and shape controllable, while lithium intercalation techniques[12] suffer from physical and electronic changes to the crystal structure. Chemical vapor deposition (CVD) has recently been found to be successful at producing large-area MoS_2,[13−15] but the technique requires high process temperatures in the range of 650−1000 °C and long growth times. It is also more challenging to obtain crystalline atomically thin MoS_2 with controlled number of layers by CVD.[16] Consequently, there is growing focus toward alternative synthesis methods for ultrathin MoS_2, particularly on insulating substrates such as alumina and mica.[17] However, information and studies on the growth of few-layer MoS_2 using metal substrates are still severely limited. The use of insulating substrates is necessary for studying the electronic properties of MoS_2, but metal substrates have their own set of advantages, including but not limited to a reduction in growth temperatures and the ease of producing metal−semiconductor contacts without film transfer. Furthermore, increasing evidence suggests that hybridizing MoS_2 with metallic materials can lead to their superior performance as electrocatalysts for the hydrogen evolution reaction (HER) due to synergistic interactions. For example, the introduction of a metal support can substantially alter the H binding energy of MoS_2,[18] enabled by charge transfer from the substrate to the overlying film and through strong metal−MoS_2 interaction at the interface. This improvement in the HER activity through the use of conductive supports that promote charge-transfer kinetics was also reported for MoS_2 nanoclusters synthesized on graphene-protected 3D Ni foams[19] and reduced graphene oxide (RGO).[20] Aside from optimizing the electrical contact between the active sites and the catalyst

Received: June 13, 2014
Accepted: August 20, 2014
Published: September 9, 2014

substrate, the presence of metallic species such as Ni and Co can enhance the activity of unsaturated Mo and/or S atoms that act as the active sites for HER,[21] leading to higher intrinsic catalytic ability of the MoS_2 hybrid material. It has been proven experimentally that the active site for HER in 2H-MoS_2 is the partially sulfide-terminated Mo-edge.[22] The sulfur edges on the other hand are not catalytically active. In promoted MoS_2 nanocrystals, the incorporation of Ni or Co ions leads to a change in morphology from truncated triangle to hexagonal, with the metal ions located at the S-edges.[21] The S-edges thus become catalytically active, and there are more HER active sites in the metal-promoted MoS_2 nanocrystals compared to pristine MoS_2, resulting in their higher intrinsic catalytic ability. From these results, it can be seen that metal-supported MoS_2 films have the potential to be used as novel catalysts for hydrogen production.

In this work, we present a study on the viability of various metals to act as the growth template for few-layer MoS_2 when a limited amount of source atoms are supplied by pulsed laser deposition (PLD). Among the advantages to using PLD for thin film deposition is the ability to grow high quality films, to ablate any material, and to obtain a stoichiometric transfer of target material onto the substrate, which is especially useful in the case of composite materials such as MoS_2. While PLD has found success in the fabrication of few-layer graphene as carried out by Koh et al.,[23] it has yet to be explored as a technique for growing other 2D layered materials. Furthermore, little is known concerning the mechanism and parameters affecting film growth of MoS_2 when using energetic source atoms that may penetrate the substrate. For PLD fabricated graphene, it has been found that the film is produced via segregation of carbon atoms onto the surface after being implanted into the metal.[24] But the situation is more complicated with MoS_2 due the presence of multiple species as the source atoms, and the high chemical reactivity of sulfur with various metals.

The metals chosen as substrates in this work were Al, Ag, Ni, and Cu. Sapphire (α-Al_2O_3) substrates have been demonstrated[25] to successfully produce ultrathin MoS_2 by CVD. It would be interesting to see if similar results can be replicated using pure Al metal films and solid MoS_2 sources in PLD. Ag, Ni, and Cu were chosen for their reactivity with sulfur to form metal sulfides, which are thought to be beneficial to the growth of highly crystalline MoS_2 due to the minimal lattice mismatch between two sulfide compounds.

2. EXPERIMENTAL SECTION

Metal films of approximately 600 nm thickness were sputtered onto normal doped (n+) Si substrates. The thin film substrates were loaded in a KrF (λ = 248 nm) Lambda Physik excimer PLD system, which was subsequently evacuated to 2×10^{-6} Torr. A MoS_2 target (99.9% purity) was ablated with a 50 mJ laser energy and for a duration of 10 s to yield an estimated 5 nm thick MoS_2 film on the substrate surface. The laser frequency was set at 10 Hz for a pulse duration of 25 ns, and the laser spot size was 1 mm^2. The target was rotated at a speed of 6 rpm with the laser ablating a circular outline of 2 cm in radius. Substrate temperature was kept at 500 °C during ablation, and subsequently decreased at a controlled rate of 50 °C/min until the temperature reached 300 °C, thereupon natural cooling took over.

The as-deposited samples were characterized with a JEOL JEM-2010F transmission electron microscope (TEM) operated at 200 kV and a Renishaw Raman spectrometer 2000 with an excitation wavelength of 514.5 nm. The green Raman laser beam had a spot size of 1 μm and was focused using an optical microscope at 50× magnification. Surface composition was analyzed by X-ray photoelectron spectroscopy (XPS), using a Kratos Analytical Axis Ultra^{DLD} UHV spectrometer with a monochromatized Al Kα X-ray source (1486.6 eV) scanning a spot size of 700 μm by 300 μm. Core-level XPS spectra were obtained by photoelectrons at a takeoff angle of 15°, measured with respect to the sample surface at a vacuum of 5×10^{-9} Torr. The pass energy for the narrow scans was set at 20 eV.

3. RESULTS

Figure 1 shows the Raman spectra of the as-deposited film on the various metal substrates fabricated using a laser energy of 50

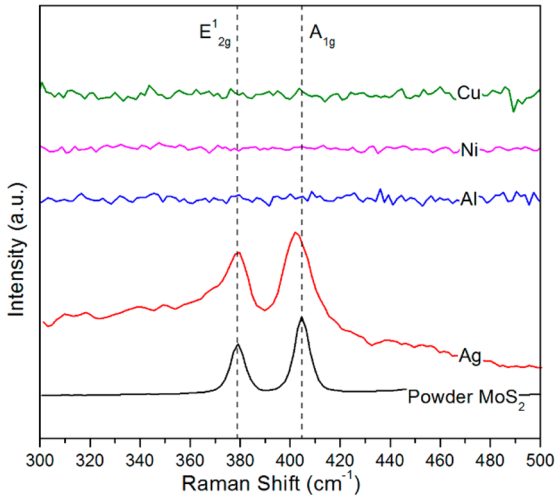

Figure 1. Raman spectra of as-grown samples fabricated on different metal substrates. Left and right dashed lines indicate the positions of the E^1_{2g} and A_{1g} peaks in bulk MoS_2 respectively.

mJ and a deposition time of 10 s. Also included for comparison is the spectrum of powder MoS_2, consisting of two peaks at 379.1 and 404.8 cm^{-1} that correspond to the 2H-MoS_2 Raman modes of E^1_{2g} and A_{1g}, respectively.[26] The in-plane E^1_{2g} mode is associated with the opposite vibration of two S atoms with respect to the Mo atom in the $x-y$ plane, while the out-of-plane A_{1g} mode results from vibration of only S atoms in the z-direction of the unit cell.[27] The presence and intensity of these two peaks are indicators of the crystallinity of MoS_2. Based on the Raman spectra of our samples, it appears that only Ag was successful in forming crystalline MoS_2 at this deposition parameters, while the Mo and S atoms on other metal substrates either form a more disordered structure or a separate compound altogether.

For ultrathin MoS_2 with $\leq$4 layers, the E^1_{2g} band blue-shifts while the A_{1g} vibration red-shifts with decreasing layer thickness.[28] The shift in the A_{1g} peak is attributed to stronger interlayer van der Waals forces with increasing thickness, caused by the influence of neighboring layers that suppress atom vibration.[29] For the shift in the E^1_{2g} mode, it is suggested that stacking induced changes in structure or increased dielectric screening of long-range Coulomb interactions in multilayer MoS_2 are more dominant factors. These shifts in Raman peak positions allow reliable identification of layer thickness in MoS_2 samples with less than five layers. For our MoS_2 on Ag samples, the E^1_{2g} and A_{1g} peak positions are determined to occur at 402.4 and 380.2 cm^{-1} respectively, indicating an ultrathin film with two to three layers. A TEM image of the sample is shown in Figure 2, with few-layer MoS_2 imaged as lattice fringes with interlayer spacing of 0.65 nm on top of Ag, confirming the results from Raman spectroscopy. The interplanar spacings of approximately 0.27 nm present just

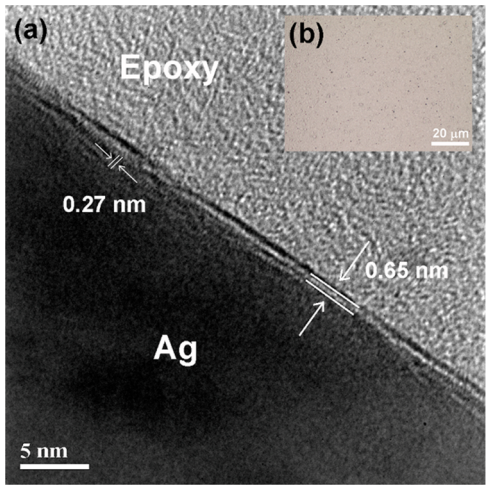

Figure 2. (a) Cross-sectional TEM image of Ag sample fabricated at 50 mJ laser energy and 10 s deposition time, showing MoS_2 lattice fringes on top of silver. Inset (b) is an overview optical image showing uniform coverage of the deposited film.

underneath the layer of MoS_2 can be ascribed to the (120) plane of monoclinic Ag_2S [JCPDS #14-0072]. As the MoS_2 sheets were grown on top of an Ag layer, the domain size of the MoS_2 crystals would follow the grain size of the underlying metal. From scanning electron microscope images, the Ag layer was determined to have an average grain size of ~600 nm, with the smallest grains having an average diameter of 150 nm.

Crystalline MoS_2 was also formed on Al when the deposition parameters was adjusted. As shown in Figure 3, the emergence

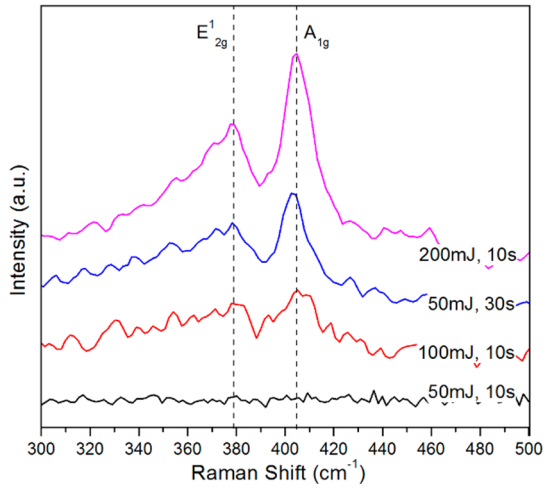

Figure 3. Raman of Al samples fabricated using different laser energies and deposition times. Left and right dashed lines indicate the positions of the E^1_{2g} and A_{1g} peaks in bulk MoS_2, respectively.

of the characteristic Raman bands at approximately 379 and 404 cm^{-1} indicate that a longer deposition time and higher laser energies impart considerable crystal ordering to the MoS_2 structure. This would suggest that a larger amount of source atoms Mo and S are required for formation of a crystalline structure on Al than is needed for Ag substrates. Compared to MoS_2 on Ag, the Raman peak intensities are much lower and the full width at half-maxiumum slightly wider for MoS_2 on Al, both indicators of multiple defects that degrade film quality. The weak Raman signal also makes quantitative analysis of the number of layers in the as-deposited film difficult, particularly in the sample grown at 100 mJ laser energy. For the 50 mJ, 30 s sample, a slight blue-shift of the E^1_{2g} band can be observed, suggesting the formation of a MoS_2 film with approximately three to four layers. This is corroborated by the TEM image shown in Figure 4, in which the lattice fringes of MoS_2 are seen on top of an aluminum native oxide coating, which appears to be mostly amorphous. The TEM image also reveals that the MoS_2 film obtained is essentially semicrystalline, as predicted by the Raman spectra. Beyond a laser energy of 100 mJ, the laser fabricated MoS_2 film on Al has more than four layers as seen from the Raman peak positions.

Figure 5 depicts the XPS high resolution scans of Mo and S for films deposited at 50 mJ energy and for 10 s on Ag, Al, and Ni substrates. Two peaks at approximately 228.7 and 231.9 eV that correspond to Mo^{4+} $3d_{5/2}$ and Mo^{4+} $3d_{3/2}$ of MoS_2, respectively, are present for all three substrates. In the S 2p spectra, the known doublet peaks of the S^{2-} species in MoS_2 occurs at 161.9 and 163.1 eV, and is similarly present for all metals. This independently confirms that MoS_2 and not a different compound forms on Ag, Al, and Ni. There is an additional S 2p doublet in the Al sample located at 163 and 164.2 eV, assigned to the binding energies of apical S^{2-} or bridging disulfide S_2^{2-} ligands,[30] and can essentially be attributed to the presence of amorphous sulfur that significantly reduces the crystalline quality of MoS_2. This pattern of two doublets in the S 2p spectrum of MoS_2 deposited on Al is consistent throughout different growth conditions, and is similar to that of MoS_3.[19] The obtained film is also considerably oxidized, judging by the presence and high relative intensity of peaks consistent with Mo^{5+} and Mo^{6+} oxidation states. Compared to the Al samples, the MoS_2 on Ag substrates are of superior crystalline quality; the S 2p doublet of amorphous sulfur is absent, and the degree of Mo oxidation is much lower, with the stoichiometric ratio of S atoms to Mo calculated to be close to the ideal value of 2. The additional S 2p doublet for the Ag sample occurs at binding energies of 161.1 and 162.4 eV, which matches well with that of the S^{2-} species in Ag_2S.

The Ni samples exhibit Mo 3d scans that are similar to that of Al, but with lower relative intensities of Mo^{5+} and Mo^{6+} peaks, indicating a lower degree of oxidation. Its S 2p spectra on the other hand is a combination of the Al and Ag samples, consisting of three doublets: the first pair contributed by amorphous sulfur, the second due to the S^{2-} of MoS_2, and the final doublet appearing at 161.1 eV is within the range for metal sulfide groups. It can thus be concluded that a small amount of Ni−S phase was formed at the growth temperature of 500 °C. The obtained MoS_2 film on Ni appears to exhibit aggregation or clustering when the laser energy is increased, as supported by the development of a broad peak centered at 403 cm^{-1} in the Raman spectra of Ni (Figure 7). In the XPS scans of Cu (Figure 6), we observe that no Mo is detected in the sample, with the peak at 226 eV in the Mo 3d scan attributed to S 2s. The S 2p spectra contains two doublets, one occurring at binding energies of 161.7 and 162.9 eV and in the absence of Mo is matched to S^2 of$^-$ a Cu−S phase that forms in situ. The second doublet occurs at 168.5 and 169.7 eV, signifying the presence of oxidized sulfur species SO_4^{2-}.

4. DISCUSSION

Across the four metals tested, highly crystalline few-layer MoS_2 was formed only on Ag, but not on Al, Ni, and Cu. To understand this phenomenon, we must take into account the

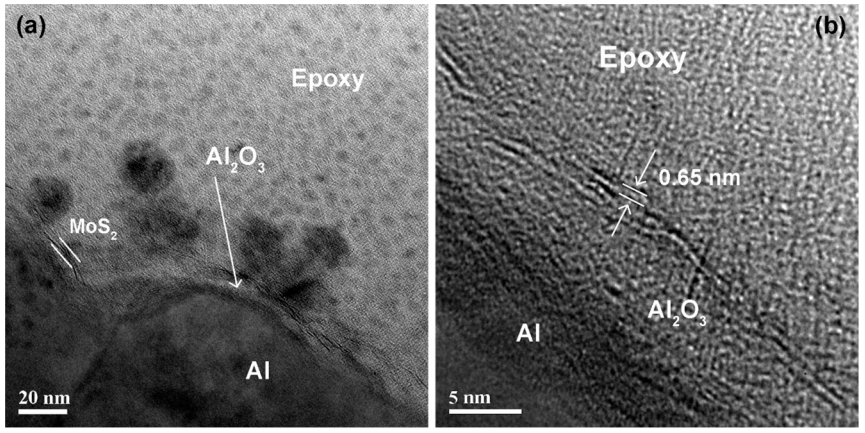

Figure 4. Cross-sectional TEM image of Al sample fabricated at 50 mJ energy and 30 s deposition time. (a) The Al metal layer is uneven and covered with an amorphous native oxide coating. (b) Lattice fringes of MoS_2 are seen above the Al native oxide layer.

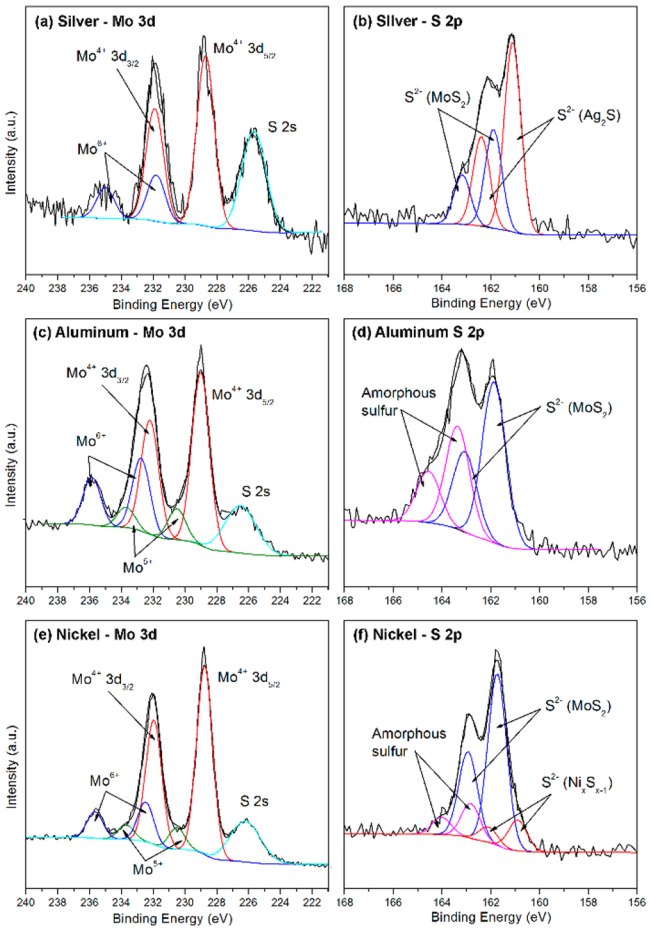

Figure 5. XPS spectra showing Mo 3d, S 2s, and S 2p core level peak regions for (a,b) Ag, (c,d) Al, and (e,f) Ni samples fabricated using 50 mJ laser energy and 10 s deposition time.

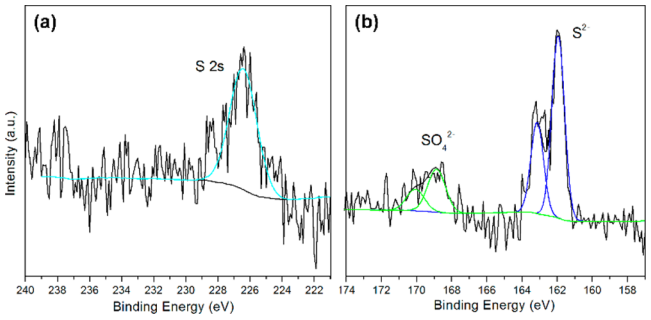

Figure 6. XPS spectra showing (a) Mo 3d, S 2s, and (b) S 2p core level peak regions for the Cu samples fabricated using 50 mJ laser energy and 10 s deposition time.

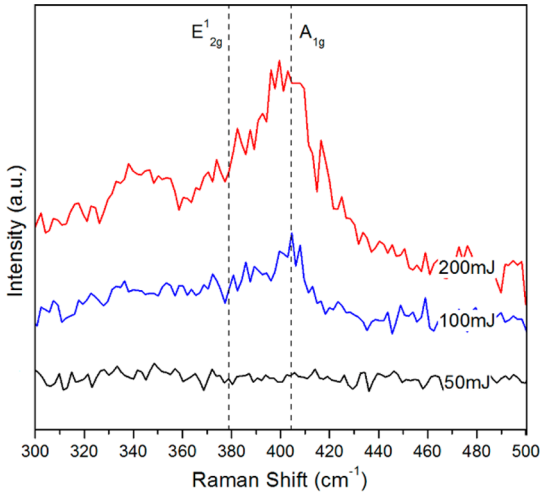

Figure 7. Raman of Ni samples fabricated using different laser energies. Left and right dashed lines indicate the positions of the E^1_{2g} and A_{1g} peaks in bulk MoS_2 respectively.

solubility and chemical reactivity of Mo and S atoms with these metals. We consider also that, with PLD, the supplied source atoms are energetic and can penetrate into the metal layer rather than simply being deposited onto the surface. In the case of silver, Mo is insoluble in solid Ag at any temperature,[31] while S reacts with Ag to form silver sulfide. During the initial growth process, chemisorption of S atoms into silver gives rise to the formation of an Ag_2S phase at the surface regions of the substrate. The relatively intense XPS signals from the S^{2-} species of Ag_2S suggests that MoS_2 is strongly interacting with the silver substrate through the formation of sulfide bonds; Mo atoms that segregate out of silver bind to the sulfur species in Ag_2S, in addition to unreacted S atoms. The energy supplied by the pulsed laser and by heating imparts mobility to the Mo and S atoms that allow them to rearrange into an orderly configuration during the subsequent cooling process. Small crystallites of MoS_2 nucleating in the first part of the

dx.doi.org/10.1021/am503719b | ACS Appl. Mater. Interfaces 2014, 6, 15966−15971

crystallization process are supported and surrounded by a soft Ag_2S phase matrix, which grants further mobility to the atoms and thus promotes grain growth. Minimal lattice mismatch (~2.6%) between the (120) plane of Ag_2S and the *b*-axis of the MoS_2 unit cell (Figure 8) further facilitates periodic ordering

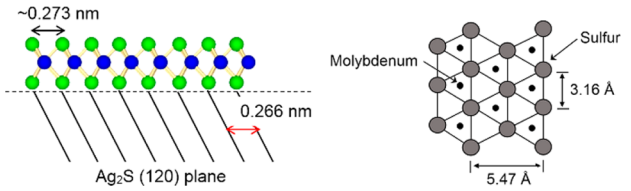

Figure 8. Schematic diagram of MoS_2 film on top of (120) plane of Ag_2S. Lattice misfit between the two is calculated to be ~2.6%.

that gives the obtained film its high crystallinity. As laser energy can be increased and cooling rate decreased to provide more energetic source atoms, the degree of crystallinity in the resulting MoS_2 film can be tuned as desired to achieve the optimum value.[32] The quality of the as-deposited MoS_2 film is believed to be minimally affected by oxide formation, which is mostly due to excess Mo atoms on the substrate surface reacting with oxygen when exposed to air. This was deduced from angle resolved XPS measurements and the calculated stoichiometric ratio of S: Mo atoms, which is close to the ideal value of 2. The crystalline quality of PLD grown MoS_2 on silver appears to be comparable to CVD grown MoS_2 sheets, with uniform coverage of layers over the entire substrate and average crystallite dimensions of a few hundred nanometers. Photoluminescence measurements of the few-layer MoS_2 film have also demonstrated pronounced signals at the direct excitonic transitions occurring at wavelengths of 615 and 670 nm,[32] indicating strong semiconducting characteristics of the 2H-MoS_2 crystal structure and a low density of defects.

Under atmospheric conditions, aluminum metal forms a passivating oxide layer with chemical formula Al_2O_3, which can be clearly observed as a bright amorphous layer in the TEM images of Al samples. Mo atoms implanted into the Al substrate subsequently interact strongly with the oxide layer through bond formation with oxygen atoms, as shown by the prominent peaks from Mo^{5+} and Mo^{6+} states in the XPS scans. As Mo atoms are initially consumed by oxide formation, there are always excess S atoms on the substrate surface that bond to each other to form elemental sulfur. Furthermore, the uneven surface of the substrate oxide layer and its mostly amorphous nature creates a high energy barrier to crystallization. On such amorphous substrates, nuclei are randomly oriented, and there is competition among crystallites in that nucleate various orientation during film growth. Consequently, coalescence does not occur as it is more favorable for crystallites to remain as islands embedded in an amorphous matrix rather than form a continuous crystalline film. This leads to the formation of a broken, semicrystalline MoS_2 film on top of aluminum. An increase in deposition time improves the crystallinity of the film slightly because the first layer of semicrystalline MoS_2 becomes part of the support/template for succeeding layers, lowering the energy barrier to crystallization. Increasing the laser energy gives rise to the same effects, in addition to imparting enhanced mobility to the atoms.

Both Cu and Ni develop native oxide coatings in air, similar to aluminum. Oxides of molybdenum are formed when Mo atoms are embedded in the Ni substrate because of the low solubility of Mo in NiO, but the adlayer−substrate interaction through the oxygen bonding is much weaker than that in the Al substrate, as deduced from the lower relative intensity of the XPS peaks from Mo oxidation states. A lower degree of oxidation means that more Mo atoms are available for reaction with sulfur, and thus, the relative intensity of the XPS peaks from amorphous sulfur is also significantly lower in comparison to the Al samples. According to the Ni−S phase diagram,[33] a Ni_xS_{x-1} phase can be in equilibrium with the solid phase with increasing sulfur content. While a Ni−S phase does form in situ, the S 2p peak corresponding to this phase is very weak, as opposed to the intense signal from S^{2-} of Ag_2S in the Ag sample. This suggests that the amount of Ni−S phase present in the sample is very low, and insufficient to act as a template for thin film growth. The Ni/NiO layer thus makes up the bulk of the surface upon which MoS_2 grows, and the resulting film is amorphous at low laser energies. With an increase in the laser energy, the MoS_2 film begins to exhibit signs of clustering due to enhanced atomic mobility and some order in the arrangement of atoms is achieved, marked by the emergence of a broad peak at ~403 cm^{-1} in the Raman spectra. Increasing the deposition time makes little to no difference, however, as clustering requires energy that must be provided by heating or from the laser. Crystallization is unable to take place owing to the relatively large lattice mismatches between the template and MoS_2, which creates large stresses in the obtained film that must be released by breaking the periodic arrangement of atoms. In the case of Cu, the formation of its characteristic patina, composed of a mixture of sulfates, carbonates and sulfides, dominates over any other reaction. This inferred from the presence of oxidized sulfur species SO_4^{2-} in the XPS scans, and an observable color change in the film from reddish to cyan. Mo has near-zero solubility in Cu, and as it is unable to bind to oxygen, all of which is consumed by the formation of the patina, the Mo atoms exists only as adsorbates on the Cu film. They are thus easily released by desorption with the thermal energy provided by heating during the deposition process, and consequently, no Mo species are detected in XPS scans.

5. CONCLUSION

We have presented the fabrication of crystalline few-layer MoS_2 on metal substrates using pulsed laser deposition. This technique involves the in situ formation of an appropriate scaffold/template for growth, and subsequent segregation of dissolved source atoms in the metal onto the surface. As such, the method is a combined physical and chemical process in which solubility and chemical reactivity of the source atoms with the underlying metal substrate are important factors affecting thin film growth. Of particular significance is the reaction of sulfur with the substrate; formation of a metal sulfide phase in situ is critical to growth of highly crystalline MoS_2. Any interactions between Mo and the substrate, however, are usually detrimental to the film quality, as this leaves excess S atoms on the surface that bind to each other to form amorphous sulfur. Despite the formation of metal sulfides in situ, both Ni and Cu failed to produce crystalline MoS_2. For either case, the sulfide formed was insufficient, in addition to being consumed to formed sulfates in the Cu substrates. In contrast, Ag was found to be very successful as a substrate for highly crystalline few-layer MoS_2 fabrication, even at low laser energies, due to the formation of substantial amounts of an Ag_2S phase. Even though alumina substrates have been

effectively utilized as epitaxial substrates for MoS_2 in CVD processes, the aluminum substrates used in this work could produce only semicrystalline few-layer MoS_2 when the growth parameters were adjusted to cater to the metal. This is partly attributed to the amorphous nature of the native oxide coating and partly to the energetic Mo atoms supplied by PLD that penetrate into the substrate, resulting in high levels of molybdenum oxide.

AUTHOR INFORMATION

Corresponding Author

*E-mail: msechcd@nus.edu.sg. Fax: +65 6776 3604.

Author Contributions

The manuscript was written through contributions of all authors. All authors have given approval to the final version of the manuscript.

Notes

The authors declare no competing financial interest.

ACKNOWLEDGMENTS

The authors T.A.J.L. and D.H.C.C. would like to acknowledge funding support from National University of Singapore WBS R284-000-123-112, and T.A.J.L. would like to acknowledge NUS research scholarship funding.

REFERENCES

(1) Castro Neto, A. H.; Guinea, F.; Peres, N. M. R.; Novoselov, K. S.; Geim, A. K. The Electronic Properties of Graphene. *Rev. Mod. Phys.* **2009**, *81*, 109−162.

(2) Lee, C.; Wei, X.; Kysar, J. W.; Hone, J. Measurement of the Elastic Properties and Intrinsic Strength of Monolayer Graphene. *Science* **2008**, *321*, 385−388.

(3) Mak, K. F.; Lee, C.; Hone, J.; Shan, J.; Heinz, T. F. Atomically Thin MoS_2: A New Direct-Gap Semiconductor. *Phys. Rev. Lett.* **2010**, *105*, 136805.

(4) Splendiani, A.; Sun, L.; Zhang, Y.; Li, T.; Kim, J.; Chim, C. Y.; Galli, G.; Wang, F. Emerging Photoluminescence in Monolayer MoS_2. *Nano Lett.* **2010**, *10*, 1271−1275.

(5) Wang, Q. H.; Kalantar-Zadeh, K.; Kis, A.; Coleman, J. N.; Strano, M. S. Electronics and Optoelectronics of Two-Dimensional Transition Metal Dichalcogenides. *Nat. Nanotechnol.* **2012**, *7*, 699−712.

(6) Radisavljevic, B.; Radenovic, A.; Brivio, J.; Giacometti, V.; Kis, A. Single-layer MoS_2 Transistors. *Nat. Nanotechnol.* **2011**, *6*, 147−150.

(7) Radisavljevic, B.; Whitwick, M. B.; Kis, A. Integrated Circuits and Logic Operations Based on Single-Layer MoS_2. *ACS Nano* **2011**, *5*, 9934−9938.

(8) Novoselov, K. S.; Jiang, D.; Booth, T.; Khotkevich, V. V.; Morozov, S. M.; Geim, A. K. Two Dimensional Atomic Crystals. *Proc. Natl. Acad. Sci. U.S.A.* **2005**, *102*, 10451−10453.

(9) Bertolazzi, S.; Brivio, J.; Kis, A. Stretching and Breaking of Ultrathin MoS_2. *ACS Nano* **2011**, *5*, 9703−9709.

(10) Coleman, J. N.; Lotya, M.; O'Neill, A.; Bergin, S. D.; King, P. J.; Khan, U.; Young, K.; Gaucher, A.; De, S.; Smith, R. J.; Shvets, I. V.; Arora, S. K.; Stanton, G.; Kim, H.-Y.; Lee, K.; Kim, G. T.; Duesberg, G. S.; Hallam, T.; Boland, J. J.; Wang, J. J.; Donegan, J. F.; Grunlan, J. C.; Moriarty, G.; Shmeliov, A.; Nicholls, R. J.; Perkins, J. M.; Grieveson, E. M.; Theuwissen, K.; McComb, D. W. Two-Dimensional Nanosheets Produced by Liquid Exfoliation of Layered Materials. *Science* **2011**, *331*, 568−571.

(11) Smith, R. J.; King, P. J.; Lotya, M.; Wirtz, C.; Khan, U.; De, S.; O'Neill, A.; Duesberg, G. S.; Grunlan, J. C.; Moriarty, G.; Chen, J.; Wang, J.; Minett, A. I.; Nicolosi, V.; Coleman, J. N. Large-Scale Exfoliation of Inorganic Layered Compounds in Aqueous Surfactant Solutions. *Adv. Mater.* **2011**, *23*, 3944−3948.

(12) Zeng, Z.; Yin, Z.; Huang, X.; Li, H.; He, Q.; Lu, G.; Boey, F.; Zhang, H. Single-Layer Semiconducting Nanosheets: High-Yield Preparation and Device Fabrication. *Angew. Chem., Int. Ed.* **2011**, *50*, 11093−11097.

(13) Lee, Y. H.; Zhang, X. Q.; Zhang, W.; Chang, M. T.; Lin, C. T.; Chang, K. D.; Yu, Y. C.; Wang, J. T. W.; Chang, C. S.; Li, L. J.; Lin, T. W. Synthesis of Large-Area MoS_2 Atomic Layers with Chemical Vapor Deposition. *Adv. Mater.* **2012**, *24*, 2320−2325.

(14) Lin, Y. C.; Zhang, W.; Huang, J. K.; Liu, K. K.; Lee, Y. H.; Liang, C. T.; Chud, C. W.; Li, L. J. Wafer-Scale MoS_2 Thin Layers Prepared by MoO_3 Sulfurization. *Nanoscale* **2012**, *4*, 6637−6641.

(15) Zhan, Y.; Liu, Z.; Najmaei, S.; Ajayan, P. M.; Lou, J. Large-Area Vapor-Phase Growth and Characterization of MoS_2 Atomic Layers on a SiO_2 Substrate. *Small* **2012**, *8*, 966−971.

(16) Ganatra, R.; Zhang, Q. Few-Layer MoS_2: A Promising Layered Semiconductor. *ACS Nano* **2014**, *8*, 4074−4099.

(17) Ji, Q.; Zhang, Y.; Gao, T.; Zhang, Y.; Ma, D.; Liu, M.; Chen, Y.; Qiao, X.; Tan, P.; Kan, M.; Feng, J.; Sun, Q.; Liu, Z. Epitaxial Monolayer MoS_2 on Mica with Novel Photoluminescence. *Nano Lett.* **2013**, *13*, 3870−3877.

(18) Chen, W.; Santos, E. J. G.; Zhu, W.; Kaxiras, E.; Zhang, Z. Tuning the Electronic and Chemical Properties of Monolayer MoS_2 Adsorbed on Transition Metal Substrates. *Nano Lett.* **2013**, *13*, 509−514.

(19) Chang, Y. H.; Lin, C. T.; Chen, T. Y.; Hsu, C. L.; Lee, Y. H.; Zhang, W.; Wei, K. H.; Li, L. J. Highly Efficient Electrocatalytic Hydrogen Production by MoS_x Grown on Graphene-Protected 3D Ni Foams. *Adv. Mater.* **2013**, *25*, 756−76.

(20) Li, Y.; Wang, H.; Xie, L.; Liang, Y.; Hong, G.; Dai, H. MoS_2 Nanoparticles Grown on Graphene: An Advanced Catalyst for the Hydrogen Evolution Reaction. *J. Am. Chem. Soc.* **2011**, *133*, 7296−7299.

(21) Merki, D.; Vrubel, H.; Rovelli, L.; Fierro, S.; Hu, X. *Chem. Sci.* **2012**, *3*, 2515.

(22) Jaramillo, T. F.; Jørgensen, K. P.; Bonde, J.; Nielsen, J. H.; Horch, S.; Chorkendorff, I. Identification of Active Edge Sites for Electrochemical H_2 Evolution From MoS_2 nanocatalysts. *Science* **2007**, *317*, 100−102.

(23) Koh, A. T. T.; Foong, Y. M.; Chua, D. H. C. Cooling Rate and Energy Dependence of Pulsed Laser Fabricated Graphene on Nickel at Reduced Temperature. *Appl. Phys. Lett.* **2010**, *97*, 114102.

(24) Yu, Q.; Lian, J.; Siriponglert, S.; Li, H.; Chen, Y. P.; Pe, S. Graphene Segregated on Ni Surfaces and Transferred to Insulators. *Appl. Phys. Lett.* **2008**, *93*, 113103.

(25) Liu, K. K.; Zhang, W.; Lee, Y. H.; Lin, Y. C.; Chang, M. T.; Su, C. Y.; Chang, C. S.; Li, H.; Shi, Y.; Zhang, H.; Lai, C. S.; Li, L. J. Growth of Large-Area and Highly Crystalline MoS_2 Thin Layers on Insulating Substrates. *Nano Lett.* **2012**, *12*, 1538−1544.

(26) Eda, G.; Yamaguchi, H.; Voiry, D.; Fujita, T.; Chen, M.; Chhowalla, M. Photoluminescence from Chemically Exfoliated MoS_2. *Nano Lett.* **2011**, *11*, 5111−5116.

(27) Li, H.; Zhang, Q.; Yap, C. C. R.; Tay, B. K.; Teo, E. H. T.; Olivier, A.; Baillargeat, D. From Bulk to Monolayer MoS_2. Evolution of Raman Scattering. *Adv. Funct. Mater.* **2012**, *22*, 1385−1390.

(28) Lee, C.; Yan, H.; Brus, L. E.; Heinz, T. F.; Hone, J.; Ryu, S. Anomalous Lattice Vibrations of Single- and Few-Layer MoS_2. *ACS Nano* **2010**, *4*, 2695−2700.

(29) Molina-Sanchez, A.; Wirtz, L. Phonons in Single-layer and Few-layer MoS_2 and WS_2. *Phys. Rev. B* **2011**, *84*, 155413.

(30) Shi, Y.; Wang, Y.; Wong, J. I.; Tan, A. Y. S.; Hsu, C.; Li, L.; Lu, L.; Yang, H. Y. Self-Assembly of Hierarchical MoS_x/CNT Nanocomposites ($2 < x < 3$): Towards High Performance Anode Materials for Lithium Ion Batteries. *Sci. Rep.* **2013**, *3*, 2169.

(31) Baren, M. R. The Ag-Mo (Silver-Molybdenum) System. *Bull. Alloy Phase Diagrams* **1990**, *11*, 548−549.

(32) Loh, T. A. J.; Chua, D. H. C. Pulsed Laser Fabricated Few-layer MoS_2 on Silver. *Chem. Phys. Lett.* **2014**, *610−611*, 284−287.

(33) Okamoto, H. Ni-S (Nickel-Sulfur). *J. Phase Equilib. Diffus.* **2009**, *30*, 123−123.